LABORATOIRE DE RECHERCHES SUR LA PHYSIQUE DES PLASMAS

A ROTATING MAGNETIC FIELD PINCH

I.R. Jones

A. Lietti

J-M. Peiry

LAUSANNE

A ROTATING MAGNETIC FIELD PINCH

I.R. Jones

A. Lietti

J-M. Peiry

Abstract

Helium gas at a pressure of 60 mTorr is contained in a discharge
tube of 4.8 cm diameter and 49 cm length which is equipped with
end electrodes and is situated within a multi-turn solenoid. The
gas is preionized by means of an axial current pulse of 9.5 Kamps
amplitude and 32 μsec duration. Following the preionization pulse,
two high power R.F. generators, each capable of delivering pulses
of 7 periods at a frequency of 3.10 Mc/s, are triggered. One genera-
tor produces an oscillating axial current in the preionized plasma
while the other induces an oscillating azimuthal current. The genera-
tors are adjusted to give equal B_θ and B_z peak amplitudes at the in-
ner wall of the discharge tube.
When the two oscillating currents are dephased by 90°, the plasma
experiences the continuous magnetic pressure exerted by a rotating
field. Streak photographs show that the plasma separates from the
tube wall and implodes towards the axis. Framing pictures show that
cylindrical symmetry is maintained during this implosion. The implo-
sion stage of the pinch is shown to be well represented by a solu-
tion of the appropriate snow plow equation.
At 1.1 μsec after the initiation of the R.F. discharge, luminosity
again appears in the region of the tube wall and stays there for the
remainder of the discharge. It is surmised that this light appears
because the current sheath which is driving the pinch returns to the
wall and subsequently flows there for the remainder of the discharge.
Measurements made of the time variation of the inductance of the
pinch support this supposition.

1. Introduction

The use of high frequency fields alone, both to confine plasma
and suppress instabilities is still in its infancy. The funda-
mental difficulty has been the lack of adequate high frequency
generating equipment of very high power. In this laboratory this
problem has been overcome to a certain extent by means of pulse
generators based on transmission lines of the lumped and continuous
varieties[1, 2, 3]. The development of these generators has allowed
a start to be made on relevant experiments in this field of study
and, in particular, on an experimental examination of the rotating
magnetic field pinch.

The stability of a plasma column confined by means of a magnetic
field which rotates in a plane tangential to the surface of the
plasma was first studied by Tayler[4] and Berkowitz et al[5]. Berkowitz
et al found that the growthrate of instabilities was bounded when
the wavelength of the deformation vanished. This was indeed an
improvement over the unbounded growthrate found when only a static
magnetic field is present. Nevertheless, in the main, the results
of these calculations were discouraging.

The above mentioned calculations dealt with a plasma of infinite
electrical conductivity. For the case of finite conductivity, a skin
is formed and there exists in the plasma successive radial layers
where the magnetic field is mainly axial or mainly azimuthal. Tuck[6]
and Allen (quoted in Ref. 4) suggested, from a purely qualitative
viewpoint, that the shear associated with this magnetic field struc-
ture would improve stability.

The literature of plasma physics contains, to our knowledge, only
two references to experimental work involving rotating magnetic
field pinches. Mention is made in Ref. 4 of work being undertaken
by Allen and Reynolds. It is not known how far along these lines
work subsequently progressed at Harwell. In the second reference,

Van der Laan[7, 8] and his colleagues report on an attempt to gene-
rate a rotating magnetic field pinch where the emphasis was laid
on examining the proposition of Tuck regarding the stabilizing
influence of the magnetic shear. Unfortunately, as a result of
initial conditions, a plasma column containing a large trapped
field was produced and this inhibited a comparison between theory
and experiment.

More complete calculations on the stability of the plasma-field
boundary by Weibel[9] and Troyon[10] which include the effect of
plasma dissipation and where the plasma is assumed to be either
near to or enclosed by a conductor have shown that the earlier
pessimistic results of Tayler and Berkowitz et al are not entirely
justified. It is found that the results of a stability analysis
depend strongly on the inclusion of the above two effects and on
the choice of plasma model to be used in the calculation. For a
collisionless plasma model, the rotating field pinch is found to
be completely stable against all modes of surface deformation
provided the frequency of rotation exceeds a certain minimum fre-
quency which is estimated to be about five times the average
transit frequency of an ion across the plasma column (in general
a frequency attainable in the laboratory).

For a fluid plasma model, on the other hand, this minimum frequency
is found to be of the order of the ion collision frequency which
is clearly considerably higher than experimentally feasible frequen-
cies. In an actual rotating magnetic field device the plasma will
pass from a state where it may be characterized as a fluid to one
where it may be considered to be an assembly of non-colliding parti-
cles. All that one demands, therefore, is that surface deformations
which arise at the initial stages of the discharge do not grow to a
disastrous level during this transition period. Calculations[11] of
instability growthrates based on the fluid model show that it is
reasonable to expect that the plasma will pass into the collision-
less domain, and hence into a stable state, without suffering
catastrophic disruption. It should be noted that the analysis of

Weibel and Troyon in no way invoke the possible stabilizing influence of magnetic shear; on the contrary, they assume a sharp plasma-field boundary.

In view of the enhanced prospects for a stable rotating magnetic field pinch implied by these calculations, an apparatus has been constructed to generate such a pinch. This apparatus is described in this paper and some experimental results obtained with it are reported.

2. The experimental apparatus

A schematic diagram of the complete experimental installation is shown in Fig. 1. A description of the individual components follows.

2.1. The discharge tube

The discharge tube, which has the form of an expanded H, is assembled from two cross-shaped pieces and one straight piece of Pyrex industrial glass tubing. The vacuum seals between the various sections are made by means of neoprene O-rings. The internal diameter of the linear section is 48 mm. Two plane aluminium electrodes fit into the discharge tube as shown and are connected to the preionization circuitry.

A hollow aluminium electrode, having the form of a truncated cone, fits snugly into each end of the linear section of the discharge tube. These electrodes serve to introduce the R.F.axial current into the preionized plasma. The minimum internal diameter of the electrodes is greater than 48 mm and consequently an unimpaired axial view of the interior of the discharge tube is possible from the outside. The distance between the ends of these electrodes is 490 mm. The return path for the axial current on the outside of the discharge tube is provided by four wide, overlapping, strips of 1 mm thick aluminium sheet which are insulated one from the other. These four strips also constitute the conductor which should,

in order to ensure average stability[9,10], enclose the plasma.
The mean radius of this return path is 62 mm. The absence of an
azimuthal conducting path should be noted.
A single layer solenoid is wound around the straight section of
the discharge tube on top of the axial current return strips. It
consists of eight parallel, insulated copper wires of 2.75 mm dia-
meter, each of which is wound 5.75 times around the tube. The total
length of the solenoid is 460 mm and its mean diameter is 73 mm.
The discharge tube is evacuated by means of a conventional vacuum
system. The base pressure is at all times $\leqslant 2 \times 10^{-6}$ mTorr. Dis-
charges are made in hydrogen and helium at filling pressures of
20, 60 and 100 mTorr.

2.2. Preionization circuitry

The gas was preionized by means of the discharge of two similar
pulse forming networks connected in push-pull to the two preioni-
zation electrodes. Each network is an LC low pass filter circuit
which can be charged and subsequently discharged into a load by
means of ignitron switching; the characteristics of the circuit
are as follows:

No of section - 4

L = 3.3 µh

C = 7.71 µf

Characteristic impedance = 0.65 Ω

Charging voltage: ± 13.0 kV

Half-height pulse duration: 44 µsec

The output of each circuit is connected to a preionization elec-
trode through a 0.7 Ω terminating resistor. The mean amplitude of
the resulting single current pulse is 9.5 Kamps. The fall-time of
the current pulse was deliberately shortened by crowbarring the
output of each network by means of ignitrons. The time constant of
the fall is 3.0 µsec and the half-height pulse duration of the crow-
barred pulse is 32 µsec.

In general there is a variable delay time, called the breakdown
time, between the switching of the pulse forming network and the
start of appreciable current flow in the gas. In the present expe-
riment this delay time was reduced to a small ($\sim$ 1-2 μsec) but
highly reproducible value by means of the following artifice. A 16
turn coil was wrapped around the leg of the discharge tube in the
vicinity of each preionization electrode. One end of the coil was
connected to the electrode and the other, via a 4.2 Ω resistor, to
ground. When the preionization circuit is triggered, current begins
to flow in this coil and gas breakdown is greatly facilitated. Sub-
sequent to gas breakdown, very little current flows in the coil due
to its higher impedance; the current flowing in the coil at break-
down is rapidly damped by the 4.2 Ω resistor. By moving the position
of the coil along the leg of the discharge tube, it was possible to
find a position where the breakdown time was a minimum.
The properties of the preionized gas have not been measured.

2.3. R.F. generators and matching circuits

The required rotating magnetic field is generated by simultaneously
producing oscillating axial and azimuthal currents in the preionized
gas. These currents are obtained by connecting high power RF genera-
tors, of the same frequency, to the conical end electrodes and to
the solenoid surrounding the discharge tube. The power levels and
the relative phasing of the generators are adjusted until the peak
amplitudes of the associated B_θ and B_z fields at the inner wall of
the discharge tube are equal and the dephasing between them is 90°.
Once this adjustment is made, the preionized plasma experiences the
continuous magnetic pressure of a rotating magnetic field.
The technique of adjusting the generators will be described in a
later section of this paper. This section is devoted to a descrip-
tion of the generators themselves and of the method for coupling
them to the plasma.

2.3.1. R.F. generators

The construction of the generators follows the design first described by Keller[3]. The principle of operation of this type of R.F. generator may be briefly recapitulated by reference to Fig. 2. The generator consists of two parts: a part which is called the "active part" and which consists of a number of homogeneous $\lambda/4$ line sections successively connected in series by means of spark gaps and, secondly, a part which is a continuous line of the same total length as that of the active part. The two components are connected together by means of a spark gap. Initially all the sections of the active part are charged to an equal voltage, $- V$. The continuous delay line is charged to $+ V$. At time $t = 0$ the first spark gap is switched; this produces two wavefronts which propagate in opposite directions. One of them reaches the second spark gap after a time $t = (1/4) T$ where T is the period of the square wave which will be produced. This wave front reflects at the second spark gap which is allowed to remain open. At time $t = (3/4) T$, the second spark gap is closed; this produces two new wave fronts, one of which reaches the third spark gap at time $t = (4/4) T$. Then the third spark gap is triggered at $t = (6/4) T$ and so on. The spark gaps are thus successively fired at intervals of $(3/4) T$. At the output of the generator one obtains a train of square waves of amplitude $V/2$ and period T, the number of periods is equal to the number of spark gaps.

In practice the homogeneous $\lambda/4$ line sections are approximated by LC lumped parameter sections and, furthermore, Keller[3] has shown that the continuous delay line may be replaced by an LCR compensation circuit. The generator used in this experiment incorporated both these modifications to the ideal generator; its circuit diagram is shown in Fig. 3. The circuit diagram shows two $\lambda/4$ sections. In fact the generator possessed seven such sections and could thus provide seven periods of oscillating current. Four generators were used, two to supply the axial R.F. current and two to induce the azimuthal R.F. current.

The successive triggering of the generator spark gaps at intervals of $(3/4)$ T is accomplished by means of an auxiliary synchronizing line the circuit of which is shown in Fig. 4. An initial external pulse triggers a spark gap causing the first capacitor in the synchronizing line to be discharged. This produces, firstly, four synchronous pulses which are transmitted to the generators (one pulse to trigger the first spark gap of each generator - the E_1 pulse of Fig. 3) and secondly, a pulse which after being suitably delayed, triggers the second spark gap in the synchronizing line. The discharge of the second capacitor produces four synchronous E_2 pulses plus the pulse which triggers the third spark gap, and so on. Dephasing between the generators is achieved by additionally delaying the two of the four E_1, E_2, E_3... pulses which go to the R.F. Z-generators. By delaying these two pulses by $(T/4)$, the phase of the Z-generators can be made to lag that of the θ-generators by 90°.

2.3.2. The matching circuits

The transfer of energy from the generators to the plasma has to be considered carefully. The plasma offers an impedance to the generator which is mainly inductive with a small resistive component. To obtain an efficient power transfer it is clear that the inductances of both the plasma and the solenoid must be combined with capacities to form resonant circuits which should be matched, both in frequency and impedance, to the generators.

The design of suitable resonant circuits is very much complicated by the fact that both the inductance and the resistance of the plasma vary in time and that the transfer of energy is a transient rather than a steady state process. In the present experiment extensive simplifying assumptions were made in designing the matching circuits. Steady state operation was assumed. The plasma and solenoid inductances and the plasma resistance were assumed to be constant circuit elements; the inductances were calculated on the basis of a completely plasma-filled discharge tube and values for the plasma resistance were taken which were based partly on an informed guess and partly on previous experience with similar apparatus.

Energy transfer under transient conditions has recently been considered by Weibel and Keller[12].

Axial current circuit

The two generators supplying the axial current are connected to the R.F. end electrodes in push-pull as shown in Fig. 5a. L represents the inductance of the plasma column between these electrodes and R represents the plasma and electrode sheath resistance. $(L_1 + L_2)$ is the parasitic inductance of one half of the symmetrically designed matching circuit and C is the resonating capacitor. In the high-Q limit, frequency and impedance matching between generator and load is achieved if:

$$f^2 = \frac{1}{4\pi^2 C\left[L_1 + L_2 + (L/2)\right]}$$

and

$$R_G = \frac{1}{2\pi^2 f^2 C^2 R}\left[\frac{L_1 + (L/2)}{L_1 + L_2 + (L/2)}\right]^2$$

where f is the frequency of the generator (3.10 Mc/s) and R_G is its impedance (4Ω). The following are the values used in the axial current circuit:

$$C = 90 \times 10^{-9} \text{ F}$$
$$L = 21.4 \times 10^{-9} \text{ H}$$
$$L_1 = 15.5 \times 10^{-9} \text{ H}$$
$$L_2 = 3.8 \times 10^{-9} \text{ H}$$
$$R = 0.125 \text{ Ω (assumed)}$$

Azimuthal current circuit

Fig. 5b shows the circuit diagram of the azimuthal current matching circuit. L is the inductance of the solenoid which surrounds the discharge tube and R is the transformed plasma resistance. $C_{||}$ and C_s are the resonating capacitors. Again in the high-Q limit, frequency and impedance matching is obtained if:

$$f^2 = \frac{1}{4\pi^2 L \left(C_{\parallel} + C_s\right)}$$

and

$$R_G = 2R\left[\frac{C_{\parallel} + C_s}{C_s}\right]^2$$

where f and R_G have the same meaning as above.

The circuit element values chosen were:

$$L = 260 \times 10^{-9} \text{ H}$$
$$C_{\parallel} = 4.0 \times 10^{-9} \text{ F}$$
$$C_s = 6.0 \times 10^{-9} \text{ F}$$
$$R = 0.7 \ \Omega \ \text{(assumed)}$$

Note that in this circuit the generators are connected in parallel across the load.

The constructional details of the matching circuits are shown in Fig. 6. The resonating capacitor for each half of the axial current circuit ($C = 90 \times 10^{-9}$ F) consists of an assembly of 36 ceramic capacitors mounted in parallel within a large aluminium box. An effort was made to keep the parasitic inductance of this assembly to a minimum. There are two such boxes and these provide the basic mechanical support for the discharge tube. The discharge tube is connected to the boxes by means of flexible copper diaphragms. Power transmission cables from the R.F. generators enter each box and feed the circuit at the appropriate impedance matching point. The azimuthal current circuit resonating capacitors are supported on a table placed between the aluminium boxes and are distributed symmetrically about the solenoid in order to prevent magnetic field distortion. Parasitic electromagnetic radiation in the laboratory is minimized by totally enclosing both matching circuits with conducting sheets.

3. Measurement of the rotating magnetic field

In order to produce a circularly rotating magnetic field at the inner wall of the discharge tube it is necessary to adjust both the power levels and the dephasing of the R.F. generators. A system capable of measuring directly the properties of a rotating magnetic field was constructed and carefully calibrated and was found to greatly facilitate this process of adjustment. The apparatus, a detailed description of which will appear elsewhere, consists of:

(i) A double magnetic probe which can be inserted into the discharge tube and which measures simultaneously the axial (B_z) and azimuthal (B_θ) components of the rotating field. This probe was calibrated by placing it in the uniform magnetic field region of a Helmholtz coil. The field amplitude was obtained from a knowledge of the Helmholtz coil dimensions and the value of the current feeding it. The time constants of the integrators associated with the probe were so arranged that the integrated voltage signals obtained when the probe was placed in equal B_z and B_θ fields were themselves equal to within 2.5%. The phase difference between the outputs of this double probe was also examined: for B_z and B_θ exactly in phase, the outputs were dephased by less than 1°.

(ii) Two magnetic probes external to the discharge tube which generate voltage signals proportional to B_z and B_θ. By connecting an aluminium cylinder between the two R.F. end electrodes to simulate the plasma and by placing the double magnetic probe so that it touched the inner wall of the discharge tube, it was possible to arrange that when B_z and B_θ were equal at the tube wall (as monitored by the double probe), the integrated voltage signals given by the external probes were also equal. The phase difference between the signal from an external probe and the corresponding signal derived from the double probe was reduced to zero by varying the length of the matched cable which transmitted the external

probe signal to the Faraday cage containing the oscillos-
copes. When calibrated in this manner, these external pro-
bes supersede the double magnetic probe as far as measure-
ment of B_z and B_θ at the wall of the discharge tube is con-
cerned. This is highly desirable since it was found during
the course of this experiment that in the presence of a
plasma, the internal probe, when placed near the wall, per-
turbs the B_z and B_θ fields by different amounts and thus no
longer provides even a faithful relative measurement of
these quantities.

(iii) An electronic squaring system which consists of two recti-
fying circuits, two non-linear diode circuits which actually
perform the squaring process and a summation circuit. This
squaring system can be used with either the double magnetic
probe or the two external magnetic probes. It has three out-
puts which yield respectively, a signal proportional to B_z^2,
a signal proportional to B_θ^2 and a signal which is propor-
tional to the square of the amplitude of the vector sum of
B_z and B_θ (to B^2, say).
This last signal is, of course, proportional to the magnetic
energy density of the magnetic field.

4. Generation of a rotating magnetic field pinch

R.F. discharges were made in preionized hydrogen and helium. The
R.F. generators were always triggered 9 μsec after the crowbarring
of the preionization. Although the dynamical behaviour of both
plasmas was similar, the motion of the helium plasma was slower
and better defined than that of the hydrogen plasma. Attention
was consequently directed mainly towards discharges in helium;
the results which follow refer uniquely to discharges in helium
at an initial filling pressure of 60 mTorr.
The first experiment carried out with the apparatus was an exami-
nation of the effect of various combinations of R.F. current

amplitudes and phase on the dynamical behaviour of the plasma.
The gross radial motion of the plasma was observed by means of
a frame/streak image converter camera (EL 085/IPP, Garching bei
München) sighted axially along the discharge tube. Four combina-
tions of amplitude and phase were studied and the corresponding
four sets of results are shown in Fig. 7a, b, c, d.
The trace identity and sensitivity values are as follows:

Upper trace: B_z at inner wall of
the discharge tube $\qquad$ 4.25 Kgauss/vertical division
as measured by an $\qquad$ 0.5 μsec/horizontal division
external probe

Middle trace: B_θ at inner wall of
the discharge tube $\qquad$ 4.25 Kgauss/vertical division
as measured by an $\qquad$ 0.5 μsec/horizontal division
external probe

Lower trace: B^2 output of squa- $\qquad$ 3.6 $(Kgauss)^2$/vertical division
ring circuit when $\qquad$ for Fig. 7a, b and d
the above signals $\qquad$ 9.0 $(Kgauss)^2$/vertical division
are connected to $\qquad$ for Fig. 7c
the inputs $\qquad$ 0.5 μsec/horizontal division

Streak photograph: Diameter of discharge tube = 48 mm
$\qquad\qquad\qquad$ Sweep speed shown below each photograph

The oscilloscope traces and streak photograph for each set have
been lined up so that their left hand edges correspond to the
same instant of time.

The magnetic field configurations produced in these four cases
are classified in Table 1.

Table 1

Fig.	I_θ (giving rise to B_z)	I_z (giving rise to B_θ)	Phase difference between currents	Name of associated pinch
7a	-	✓	-	Alternating Z-pinch
7b	✓	-	-	Alternating θ-pinch
7c	✓	✓	0°	Alternating screw field pinch
7d	✓	✓	90°	Rotating field pinch

The generation of the alternating Z- and θ-pinches is straightfoward, one uses only the appropriate R.F. generator, the other remaining uncharged. The screw field pinch (which has recently been studied by Bobeldijk et al[13]) is produced by first adjusting the R.F. generators to give equal B_z and B_θ amplitudes at the inner wall of the discharge tube. In practice it was found that the Q-factors for the two matching circuits were different and consequently the envelope shape of the R.F. pulses differed. An attempt was made to have equality of amplitudes during the initial stage of the pulse duration. The phase difference between the currents was then changed until it became zero. The field amplitudes were monitored by either observing the B_z and B_θ signals given by the external probes or, better still, observing the B_z^2 and B_θ^2 outputs of the squaring circuit due to these signals. The current phase difference was observed by examining its influence on the B^2 output of the squaring circuit. If this phase difference is zero, then the value of B^2 returns to zero at each half cycle of the discharge currents. This can clearly be seen in the B^2 trace of Fig. 7c. The rotating field pinch is arrived at by merely changing the current phase difference from zero to 90°. In this case, the value of B^2 never returns to zero during the duration of the R.F. pulses

and the plasma experiences the continuous magnetic pressure due to
a rotating magnetic field. Again, in practice, a perfect adjustment
of amplitude and phase is hard to achieve and the B^2 signal of Fig.
7d shows oscillations superimposed upon a continuous component.

For the alternating Z-pinch, the alternating θ-pinch and the screw
field pinch, the force exerted by the magnetic field on the plasma
takes the form of a sequence of discrete impulsions, one occurring
at each half cycle of the discharge currents. The streak photographs
show an imploding luminous sheath associated with each of these im-
pulsions. The following tentative explanation is put forward to ac-
count for this phenomenon. It is surmised that each impulsion causes
a shock wave to be propagated into the plasma. This wave is closely
followed by a rarefaction wave which arises when the magnetic pressure
temporarily drops to zero; that is, imploding cylindrical blast waves
are generated at each half period of the discharge current. The ef-
fect of the rarefaction wave is to attenuate the shock before it
reaches the central region of the discharge tube. Nevertheless some
gas will be transported from the periphery of the discharge towards
the centre of the tube. It is conceivable that the observed luminous
sheaths are associated with the blast waves and the luminosity in the
centre of the tube with the collected gas.

When the field is rotating and the magnetic pressure consequently
remains at a non-zero value for a substantial portion of the pulse
duration, the corresponding streak picture (Fig. 7d) shows that the
plasma separates from the discharge tube wall and implodes towards
the axis at a much slower rate than the luminous sheaths referred to
above. This gross detachment of the plasma from the wall and the sub-
sequent formation of a well-defined luminous column constitutes the
rotating magnetic field pinch.

5. Some measurements on the rotating magnetic field pinch

5.1. Streak and framing photographs

Fig. 8 shows a streak photograph of a rotating field pinch in helium at an initial pressure of 60 mTorr. Below it is shown a row of framing camera pictures. These are not successive photographs of a single discharge but are ones selected from a number of three-picture runs. Since the discharges were repeatable in their characteristics, these framing pictures show faithfully the progress of a typical rotating field pinch.

In the streak photograph the outer edge of the imploding plasma is interpreted as the boundary between magnetic field and plasma and the inner edge is considered to define the position of a shock wave. There is clearly an inward acceleration of the plasma during the implosion stage. The shock wave takes about 0.9 µsec to reach the centre of the tube. It should be noted that as the diameter of the plasma decreases, the amplitude of B_θ at the plasma surface increases while that of B_z remains constant. The rotating field at the plasma surface thus becomes increasingly more elliptic as the plasma contraction progresses. The light modulation seen on the imploding plasma is believed to be caused by the resulting oscillating surface magnetic pressure. The observed modulation frequency agrees with that predicted by this hypothesis (viz. twice the discharge current frequency). The light which appears at the discharge tube wall towards the end of the implosion stage is discussed in a later section of this paper. After the shock has reached the centre of the tube a well-defined plasma column of about 10mm diameter is formed which remains for 0.8 µsec before it expands to the discharge tube wall.

The framing pictures show that cylindrical symmetry is maintained by the plasma throughout its period of compression.

5.2. Dynamics of the rotating field pinch

The implosive motion of fast Z- and θ-pinches has been found to be well represented by a solution to an approximation of the hydrodynamic

equations known as the "snowplow" model (see e.g. Ref. 14). The snow-
plow model assumes that all the mass overtaken by the imploding hydro-
dynamic shock is compressed into an infinitely thin layer immediately
behind the shock so that the driving magnetic piston (the contact sur-
face) and the shock are the same interface. The rate of momentum change
of the plasma layer, balanced against the driving magnetic pressure,
then gives the inward velocity of the layer as a function of time.
Clearly this model is only valid in the strong shock limit. The snow-
plow equations were integrated numerically for the case of a rotating
magnetic field pinch in helium at a filling pressure of 60 mTorr. Due
consideration was paid to the increase of B_θ with decreasing plasma
radius. Details of this calculation will be given elsewhere. Fig. 9
shows a comparison between the observed and calculated trajectories of
the imploding plasma layer. It should be borne in mind that there are
no adjustable parameters involved in the calculations once the initial
mass distribution in the tube has been fixed. The agreement is remar-
kably good and furnishes further evidence that we have observed a
gross motion of the plasma away from the inner wall of the discharge
tube.

5.3. Inductance measurements

The streak photographs of the rotating field pinch show that towards
the end of the implosion stage light again appears in the region close
to the tube wall and stays there for the remainder of the R.F. dischar-
ge. The increase in luminosity is believed to be associated with the
production of conducting material at the wall and a subsequent growth
of currents in this material. The conducting layer screens off the
magnetic fields from the central plasma column which, in the absence
of a confining pressure, starts to expand. The non-linear interaction
between the expanding plasma column and injected wall material can
clearly be seen on all the streak photographs.
Support for this hypothesis is provided by measurements that were
made of the relative variation of plasma inductance with time. Re-
ferring to Fig. 5a, let V be the voltage measured between the points
marked 1 and 2. This voltage is given by

$$V = \frac{d}{dt} (LI_z) + I_z R$$

where L is the sum of a constant, substantial fraction of L_1 and half the inductance of the coaxial plasma system, and R is one half of the plasma resistance. We may safely assume that the plasma resistance drops quickly to such a value that the $I_z R$ term may be neglected so that

$$V = \frac{d}{dt} (LI_z)$$

It follows that the value of L at any time t, when the current is $I_z(t)$, is given by

$$L(t) = \frac{1}{I_z(t)} \int_0^t V(t') \, dt'$$

It should be noted that a variation of L with time is due solely to a variation of the inductance of the coaxial plasma system.

The voltage V was measured during a rotating field pinch by means of a resistive divider. The voltage probe signal was integrated using an RC circuit prior to being displayed on an oscilloscope. The axial R.F. current, I_z, was measured simultaneously. Fig. 10 shows the variation of L with time. The vertical error flags indicate the root-mean-square error of five measurements while the horizontal error flags reflect the fact that mean values of L were determined for each half cycle.

The variation of L with time is interpreted as follows. At the start of the R.F. discharge, the electrical conductivity of the plasma is relatively low and the skin depth is a considerable fraction of the discharge tube radius. As the discharge progresses, the temperature of the plasma rises, the skin depth becomes smaller and the value of L drops. This process occurs during the time (marked A in Fig. 10) when the external magnetic pressure has not yet produced an observable plasma motion. As soon as the plasma starts to contract, the inductance increases and continues to do so until the production of

a conducting layer at the tube wall causes the value of L to drop once more; this period is marked B in Fig. 10. After current flow has been established at the wall, the inductance remains at a more or less constant value for the remainder of the discharge.

The periods A and B have been indicated on Fig. 9. Inspection shows that the above interpretation is eminently reasonable.

6. Discussion

Evidence provided by the streak/framing photographs and inductance measurements, together with theoretical considerations of the pinch dynamics, suffices to establish that an observation has been made of a rotating magnetic field pinch.

The production of a conducting layer at the tube wall unfortunately limits the lifetime of the pinch and clearly constitutes the next problem to be faced in this study. The agreement of the observed plasma trajectory with that calculated on the basis of the snowplow model implies that a large fraction of the mass of filling gas which was initially near the wall partakes of the implosive motion.

The following are possible sources of conducting material:

(i)   The fraction of filling gas which does not undergo compression.

(ii)   Wall material vapourized by radiation from the central plasma column.

(iii) Gas liberated from the tube wall.

Spectroscopic studies of the conducting layer are to be undertaken in an attempt to identify its origin.

ACKNOWLEDGMENT

REFERENCES

1. WEIBEL, E.S.   (1964) Rev. Sci. Instr. 35, 173
2. LIETTI, A.   (1965) Rev. Sci. Instr. 36, 13
3. KELLER, R.   (1965) Helv. Phys. Acta 38, 328
4. TAYLER, R.J. (1957) Hydromagnetic instabilities of a cylindrical
    gas discharge. Part 5. Influence of alterna-
    ting magnetic fields. A.E.R.E Report T/R 2263
5. BERKOWITZ, J. et al (1958) Proceedings of the Second International
    Conference on the Peaceful Uses of Atomic Ener-
    gy, Geneva, Vol 31, p. 177, United Nations,
    New York
6. TUCK, J.L.   (1958) Proceedings of the Second International Confe-
    rence on the Peaceful Uses of Atomic Energy,
    Geneva, Vol 32, p.3, United Nations, New York
7. VAN DER LAAN, P.C.T. and RIETJENS, L.H.TH. (1962) Proceedings of
    the IAEA Conference on Plasma Physics and
    Nuclear Fusion Research, Salzburg, 1961,
    Nucl. Fusion 1962, Suppl. 2, 693
8. VAN DER LAAN, P.C.T. (1964) Plasma confinement by means of a rota-
    ting magnetic field. Rijnhuizen Report 64-16
9. WEIBEL, E.S. (1960) Phys. Fluids 3, 946
10. TROYON, F.S. (1966) Stability of a dense plasma confined by a
    rotating magnetic field. Report LRP 25-66
    Plasma Physics Laboratory, Lausanne,Switzerland
11. TROYON, F.S. (1967) Private communication
12. WEIBEL, E.S. and KELLER, R. (1967) Plasma Physics, (To be published)
13. BOBELDIJK, C. et al (1967) Plasma Physics. 9, 13
14. GLASSTONE, S. and LOVBERG, R.H. (1960) Controlled Thermonuclear
    Reactions, D. Van Nostrand Co., Inc., Prince-
    ton, p. 230

FIGURE CAPTIONS

FIG. 1   Schematic diagram of experimental installation

FIG. 2   Formation of R.F. pulse

FIG. 3   Generator circuit diagram

FIG. 4   Circuit diagram of synchronizing line

FIG. 5   Circuit diagrams of (a) axial current matching
          circuit and (b) azimuthal current matching circuit

FIG. 6   Mechanical construction of matching circuits

FIG. 7   Streak photographs corresponding to different field
          configurations (trace identity and sensitivity va-
          lues are given in the text)

FIG. 8   Streak and framing photographs of rotating magnetic
          field pinch

FIG. 9   Comparison of observed and calculated implosion
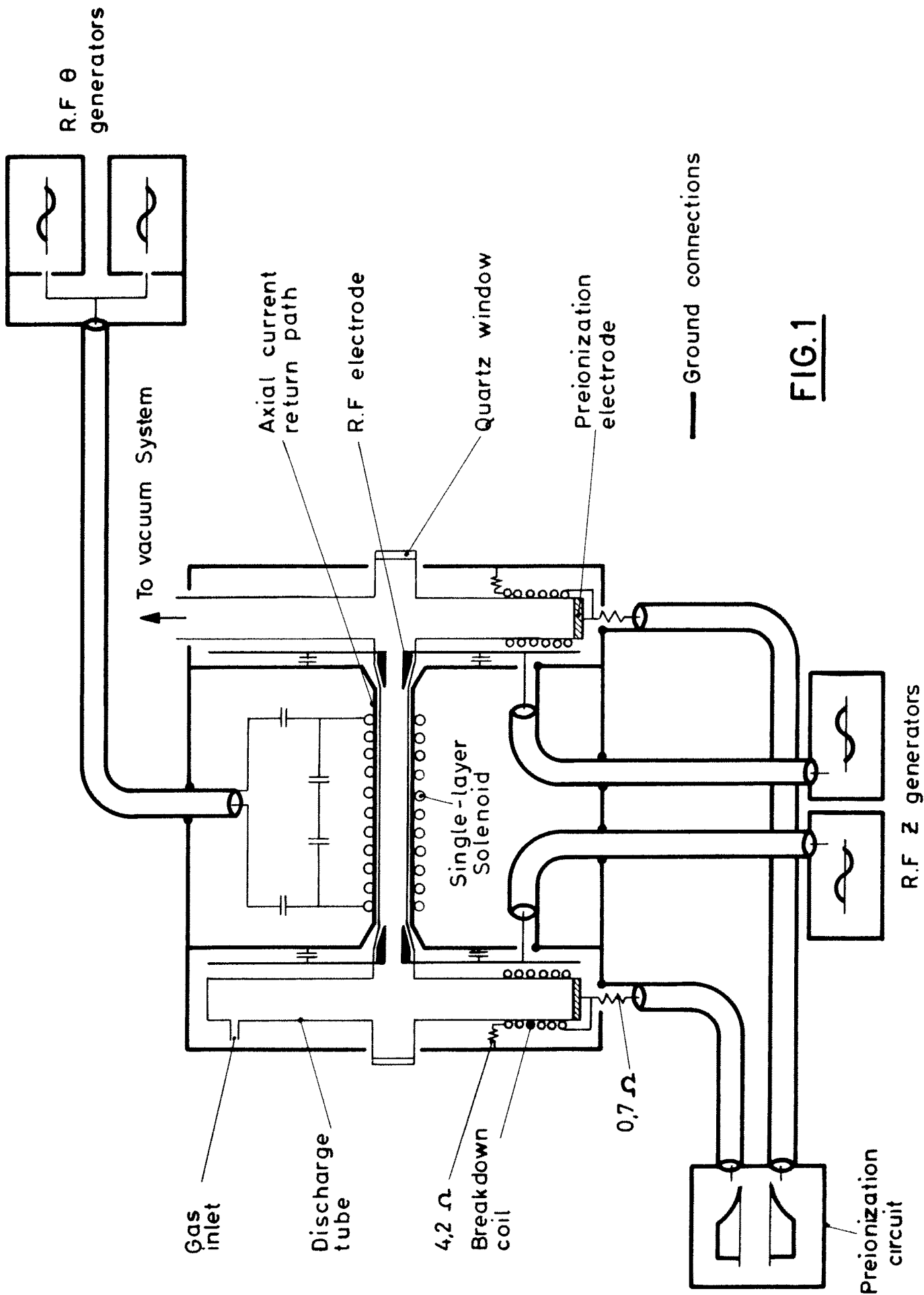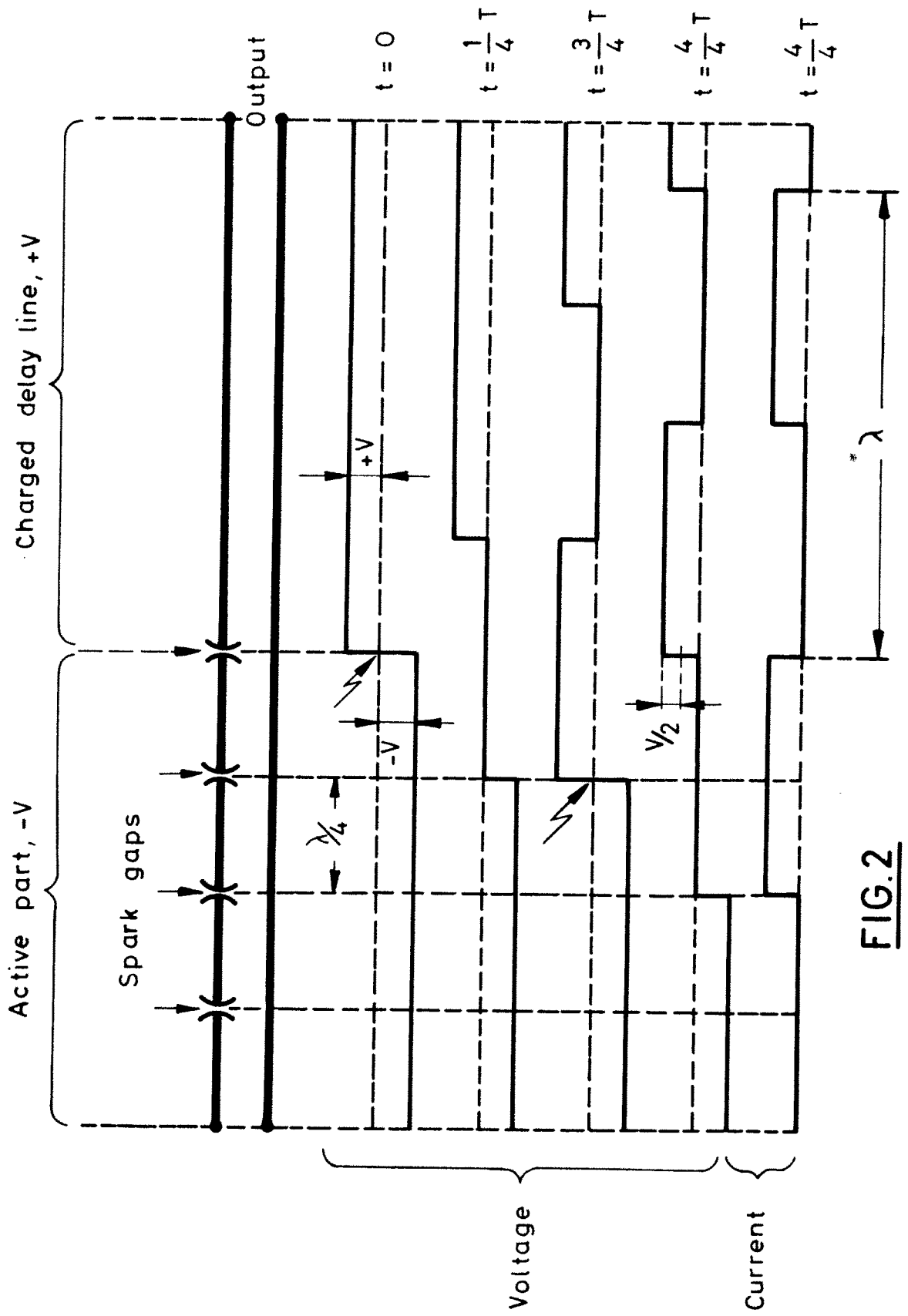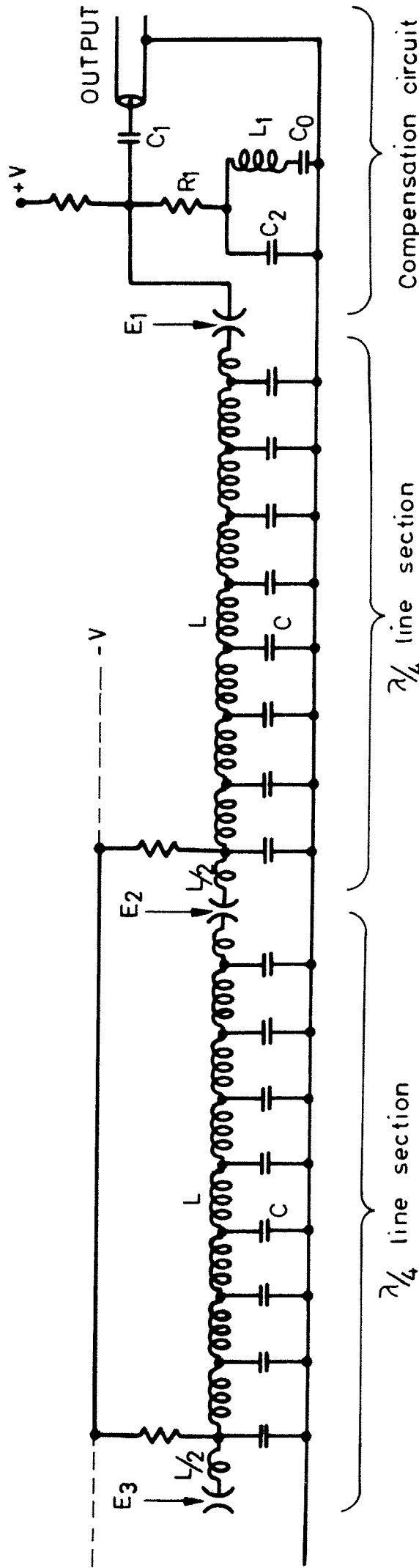   trajectories

FIG. 10   Variation of L with time

R.F θ generators

To vacuum System

Axial current return path

R.F electrode

Quartz window

Preionization electrode

— Ground connections

FIG.1

Gas inlet

Discharge tube

4,2 Ω

Breakdown coil

0,7 Ω

Single-layer Solenoid

R.F Z generators

Preionization circuit

FIG.2

OUTPUT

Compensation circuit

C_1

R_1

L_1

C_0

C_2

E_1

$+V$

$\lambda/4$ line section

$\lambda/2$

E_2

L

C

$-V$

$\lambda/4$ line section

Spark gap triggering pulses

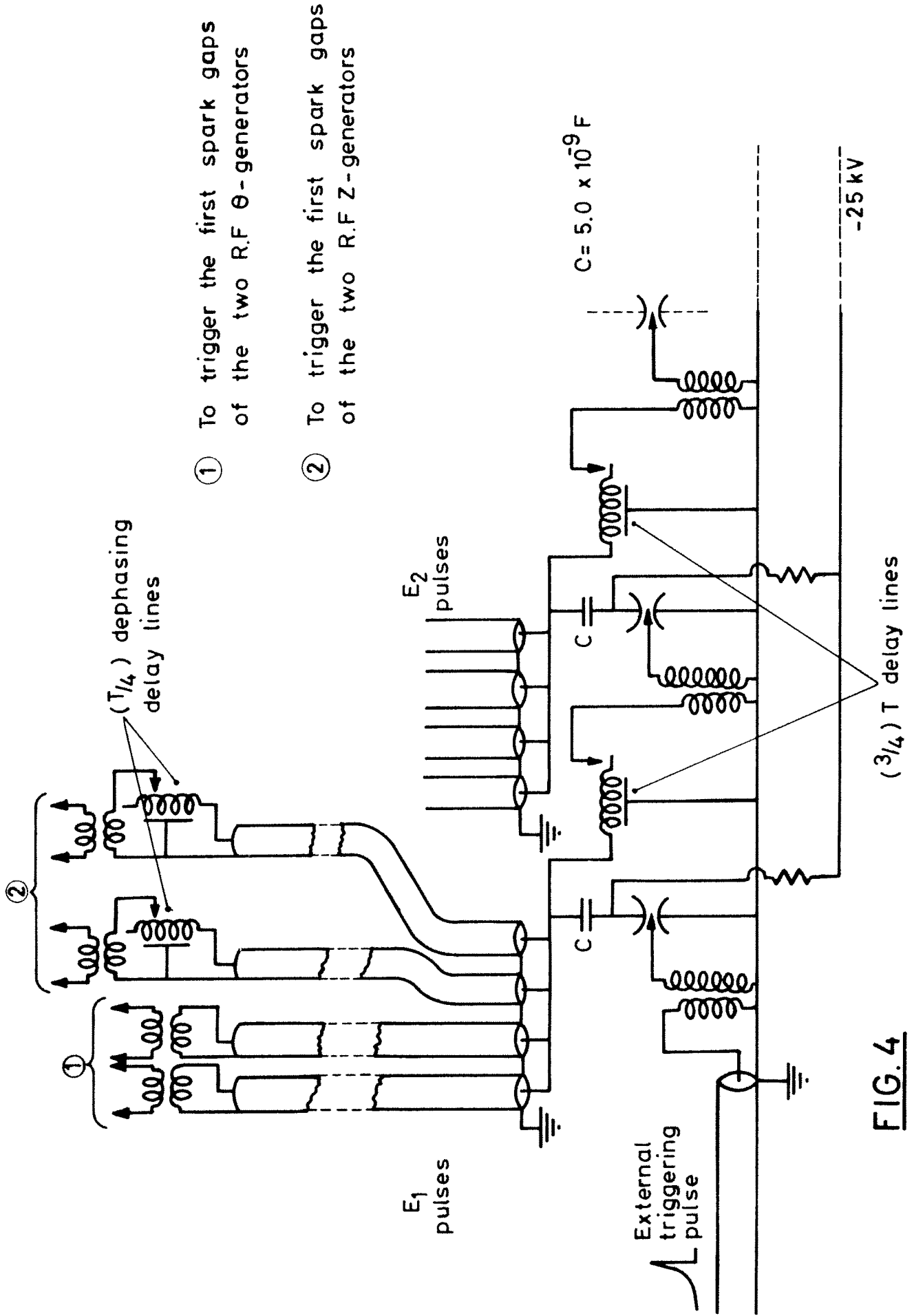$\lambda/2$

E_3

L

C

$E_1, E_2, E_3, \ldots$ Spark gap triggering pulses

$\lambda/4$ line section

Generator characteristics

Frequency = 3·10 Mc/s

Charging voltage : $\pm$ 25 kV $\longrightarrow \pm$ 35 kV

Pulse duration = 2·3 μsec

Power delivered to 4 Ω load = 50 MW
(charging voltage $\pm$ 35 kV)

Component values

$C = 2·5 \times 10^{-9}$ F

$C_0 = 1·5 \times 10^{-6}$ F

$C_1 = 2·0 \times 10^{-8}$ F

$C_2 = 1·2 \times 10^{-8}$ F

$L = 4·0 \times 10^{-8}$ H

$L_1 = 2·2 \times 10^{-7}$ H

$R_1 = 4·0 \ \Omega$

FIG.3

To trigger the first spark gaps of the two R.F θ-generators

To trigger the first spark gaps of the two R.F Z-generators

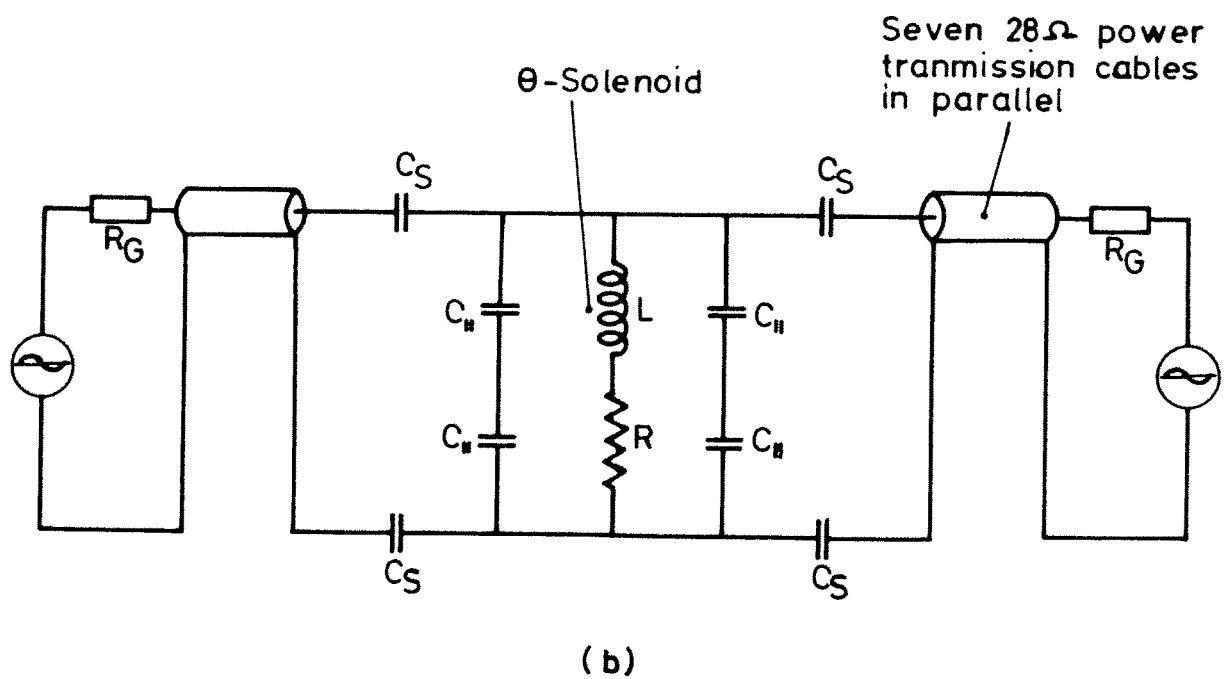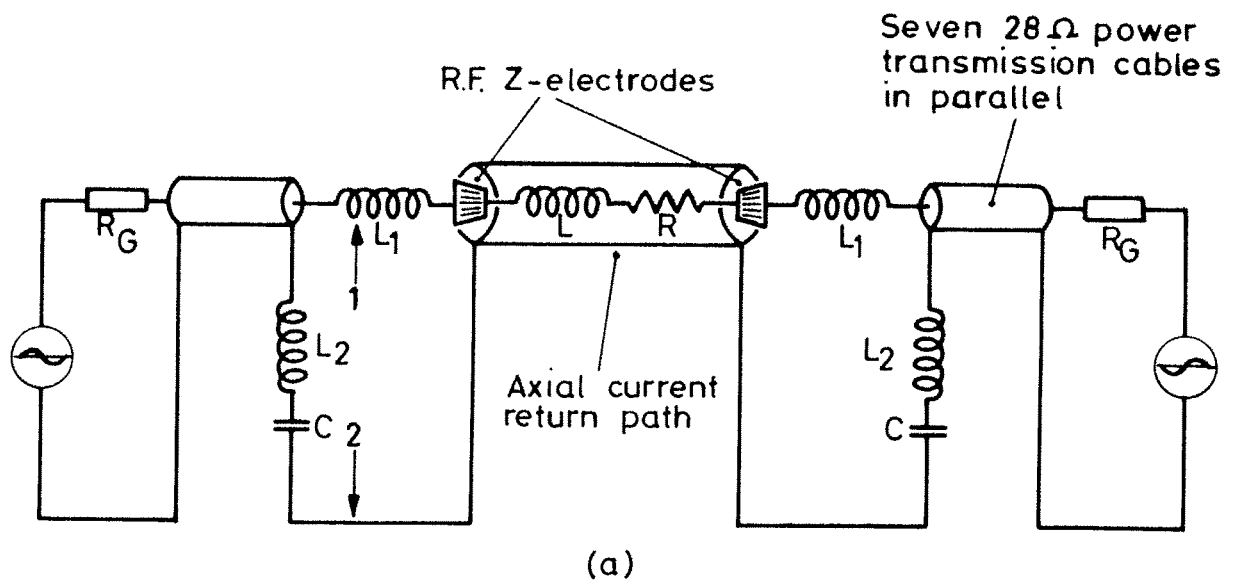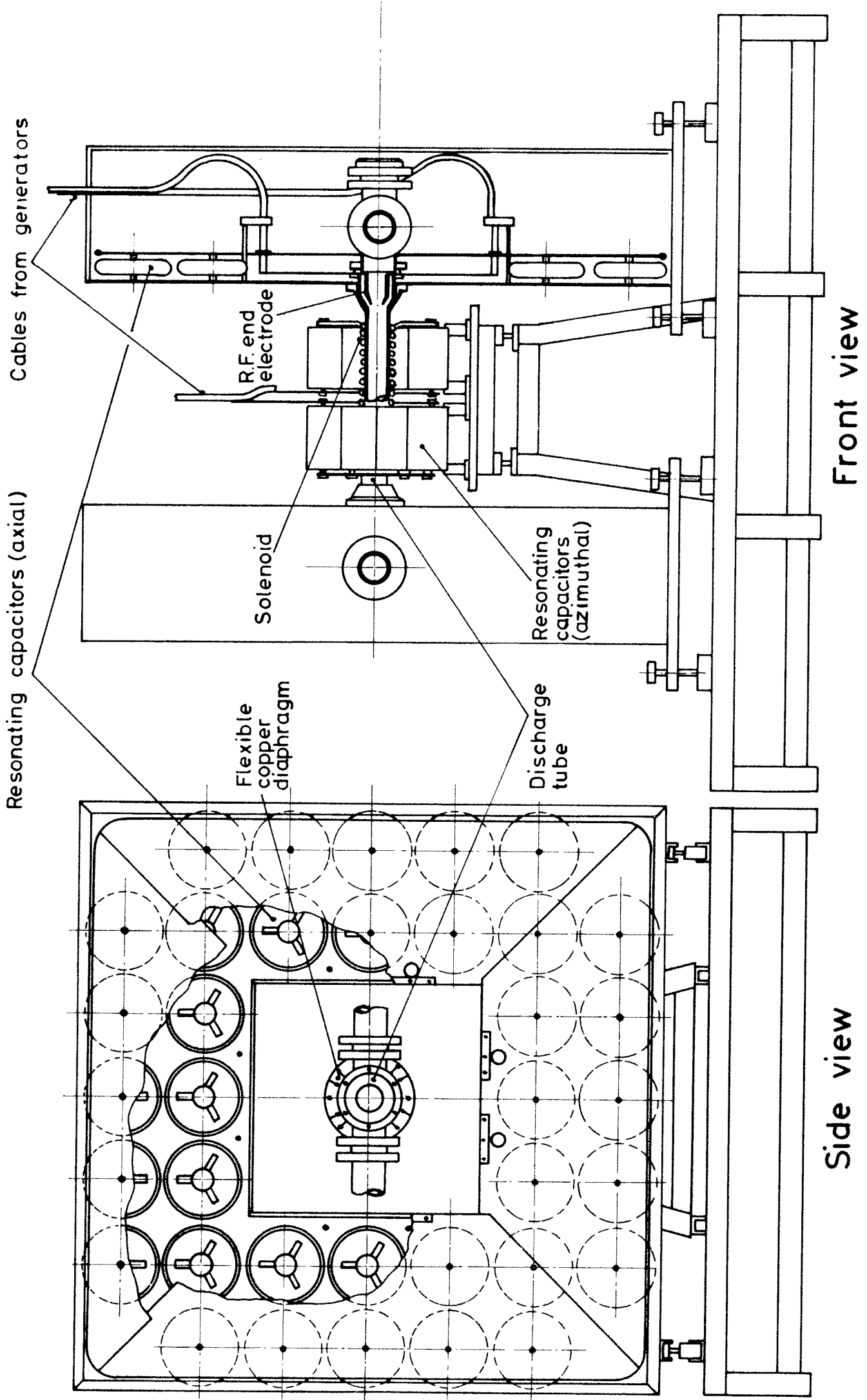① To trigger the first spark gaps of the two R.F θ-generators

② To trigger the first spark gaps of the two R.F Z-generators

$(T/4)$ dephasing delay lines

E_2 pulses

$C = 5.0 \times 10^{-9}$ F

$(3/4)$ T delay lines

E_1 pulses

External triggering pulse

C

C

-25 kV

FIG.4

(a)

(b)

F I G. 5

Cables from generators

Resonating capacitors (axial)

R.F. end electrode

Solenoid

Resonating capacitors (azimuthal)

Flexible copper diaphragm

Discharge tube

Front view

Side view

FIG.6

(a)　(b)　(c)　(d)

$\dfrac{\text{Time}}{1\,\mu\text{sec}}$

FIG.7

Start of I_z current

Diameter of discharge tube

Time $\left(\overline{1\,\mu\text{sec}}\right)$
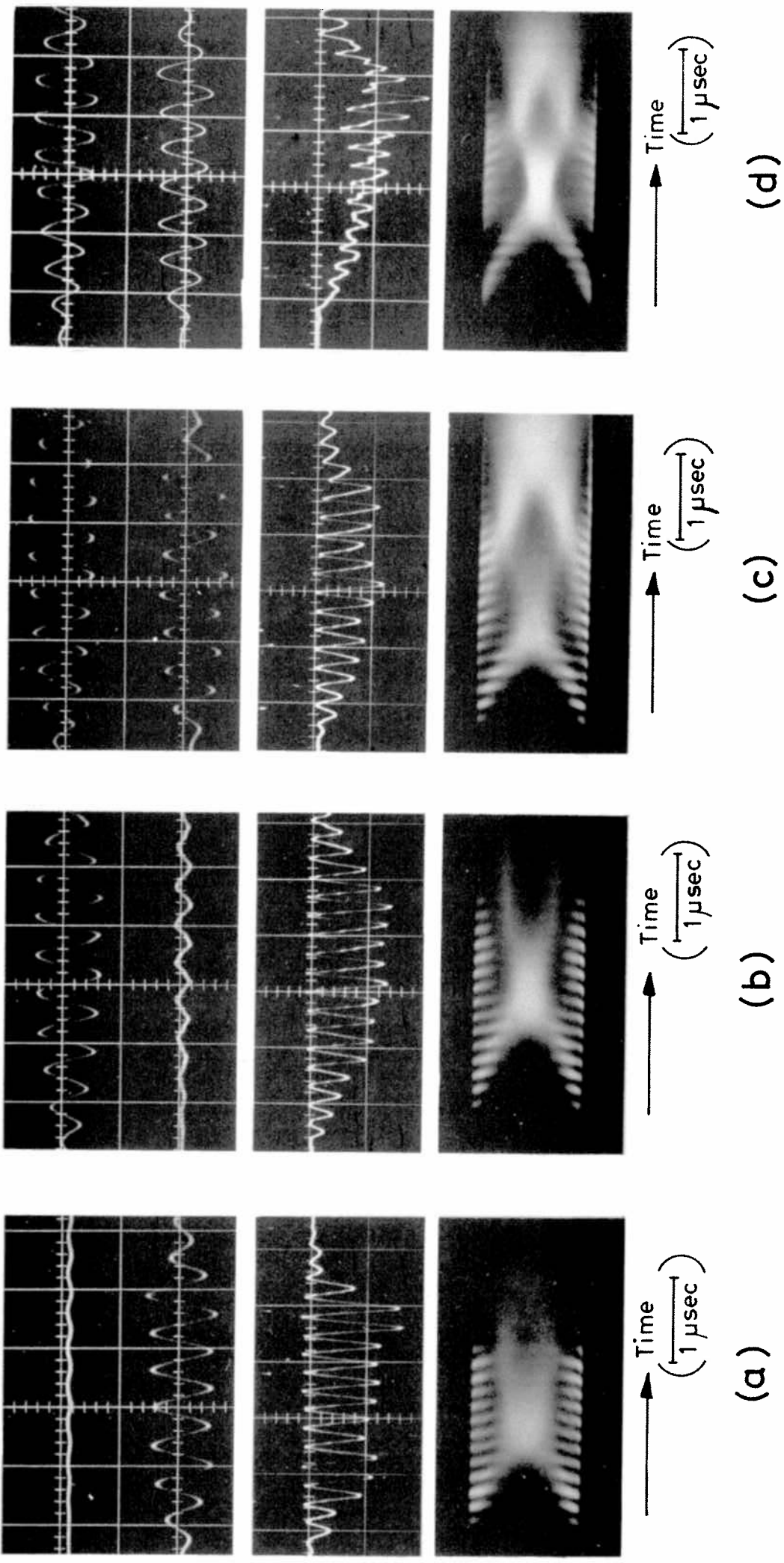
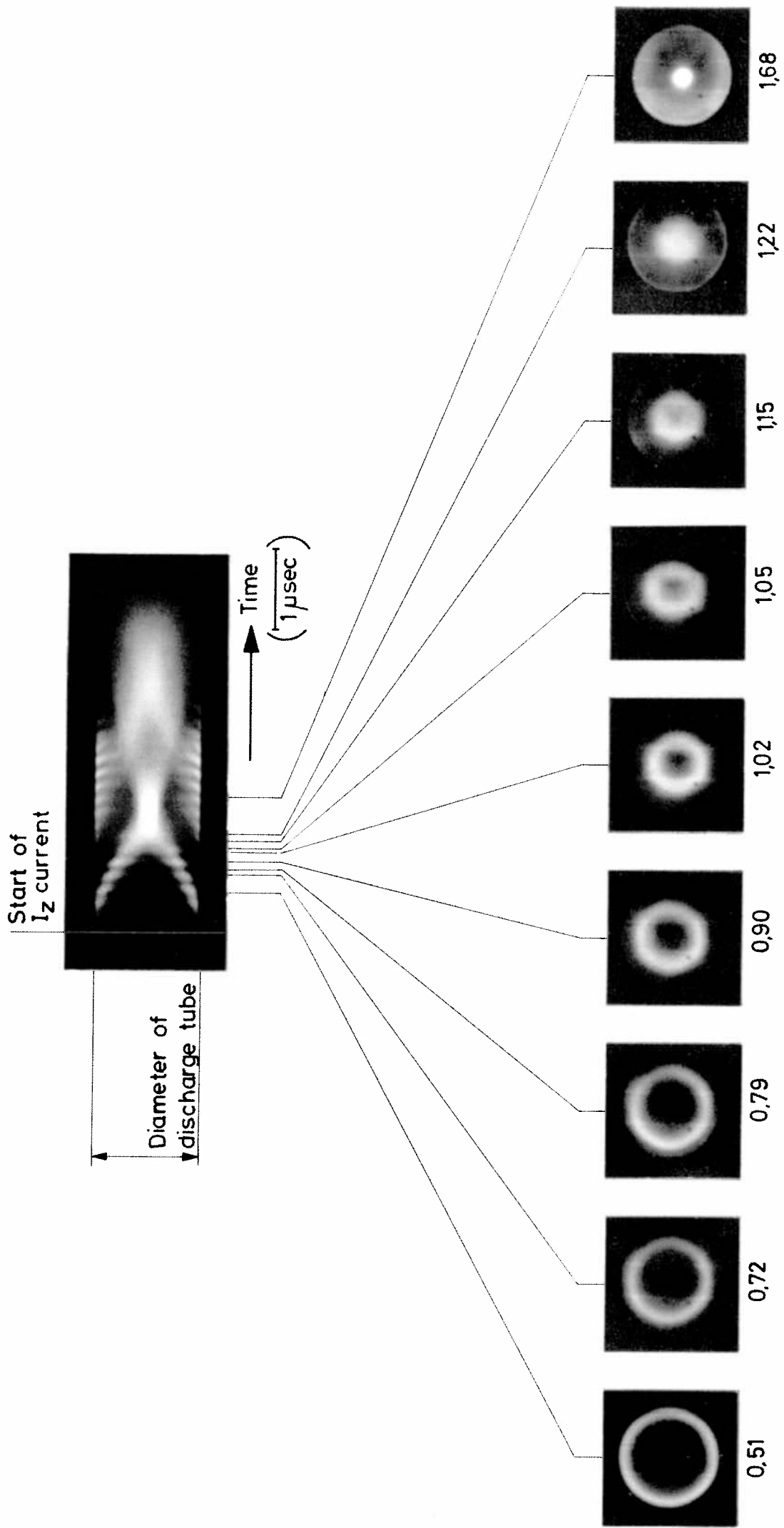0,51   0,72   0,79   0,90   1,02   1,05   1,15   1,22   1,68
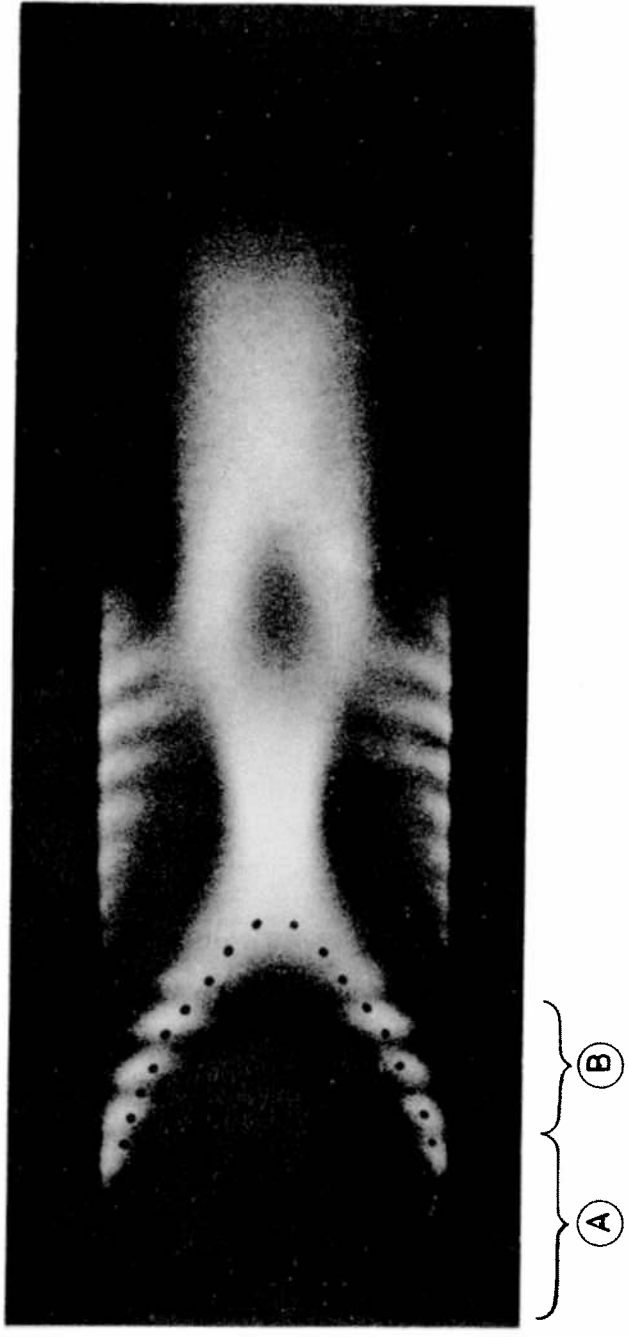
The time in microseconds from the start of
the I_z current is shown under each photograph.
The exposure time of each frame is 0,05 microsecond.
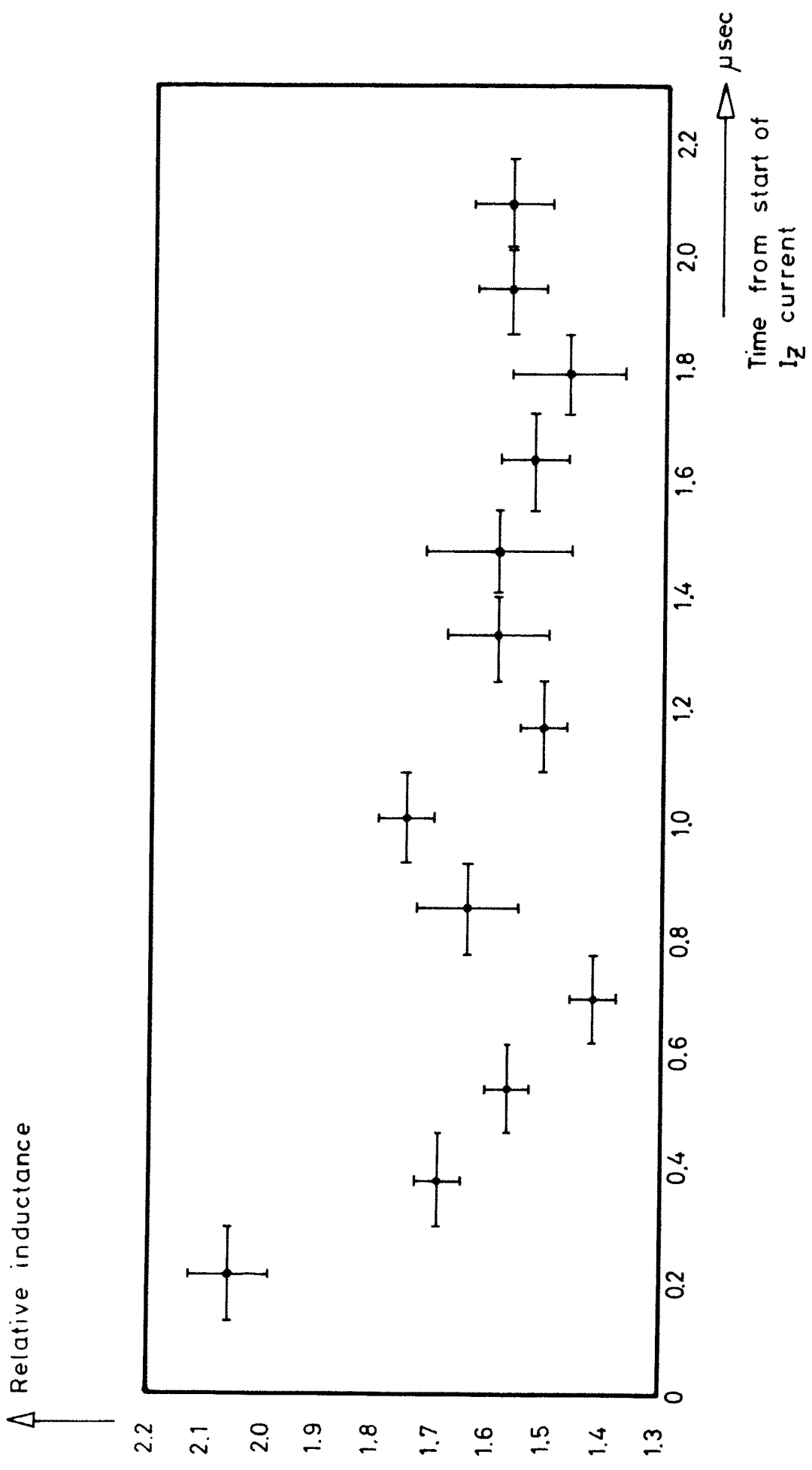
FIG. 8

······ CALCULATED TRAJECTORY

FIG.9

Relative inductance

2.2
2.1
2.0
1.9
1.8
1.7
1.6
1.5
1.4
1.3

0   0.2   0.4   0.6   0.8   1.0   1.2   1.4   1.6   1.8   2.0   2.2

Time from start of
I_z current

μ sec

Ⓐ   Ⓑ

FIG.10